INSTITUTE OF ARCHEOLOGY
AND ART HISTORY OF ROMANIAN
ACADEMY CLUJ-NAPOCA

UNIVERSITATEA TEHNICĂ
DIN CLUJ-NAPOCA

JAHA
JOURNAL OF ANCIENT HISTORY
AND ARCHAEOLOGY

editura
MEGA

Journal
of Ancient History and Archaeology

No. 12–1 / 2025

CONTENTS

ISSN 2360 266x
ISSN–L 2360 266x

Design & layout: Francisc Baja

editura MEGA

Editura Mega | www.edituramega.ro
e-mail: mega@edituramega.ro

Geanina A. BUTISEACĂ
Autonomous University of Barcelona, Institute of Environmental Science and Technology, Barcelona, Spain
Eberhard Karls Universität Tübingen, Department of Geosciences, Institute of Archaeological Sciences, Palaeoanthropology, Tübingen, Germany
butiseacageanina@gmail.com

Ovidiu ȚENTEA
National Museum of History of Romania, Bucharest, Romania
ovidiu.tentea@gmail.com

Veronika BRYCHOVA
Department of Radiation Dosimetry, Nuclear Physics Institute of the CAS, Libeň, Czech Republic
brychova@ujf.cas.cz

Iuliana VASILIEV
Senckenberg Biodiversity and Climate Research Centre, Frankfurt am Main, Germany
iuliana.vasiliev-popa@senckenberg.de

NEW INSIGHTS IN THE ROMAN COLONISATION OF DACIA: DID THE ROMAN CLIMATIC OPTIMUM INFLUENCED THE ROMAN EXPANSION IN EASTERN EUROPE?

Abstract: Records about the Roman achievements and natural events impacting their life are known from major archaeological sites around Europe, however little it is known about the climatic conditions during the Roman Empire expansion, particularly in Eastern Europe. Here we look at paleoenvironmental proxies (i.e., glycerol dialkyl glycerol tetraethers and leaf waxes) from *Colonia Dacica Sarmizegetusa*, to evaluate the general climatic conditions during the roman presence in Dacia Province. Our data indicate mean annual temperatures of ~11.5 °C, two degrees higher than the present-day temperatures in the region. The higher temperatures are associated with a decrease in C_{27} and C_{29} *n*-alkanes abundances as Roman occupancy continued, indicating an increase in deforestation around the site. The overall data show warmer and drier conditions during the Roman occupation in central Romania, suggesting a direct link between climatic conditions and Roman expansion in the area.

Keywords: *Roman Warm Period, Dacia, Colonia Dacica Sarmizegetusa, amphitheatre, sewage, biomarkers.*

1. INTRODUCTION

The maximum expansion of the Roman Empire (Ist century BC – IInd century AD) overlaps with a warming period known in the literature as the Roman Warm Period (RWP; ~200 BC – 400 AD)[1] due to the historical conjuncture and it was the warmest period in Europe in the last two millennia[2]. Here we focus on *Colonia Dacica Sarmizegetusa* (complete name *Colonia Ulpia Traiana Augusta Dacica Sarmizegetusa*) first Roman city founded in the Roman province of Dacia sometime in 108/110[3]. Despite the high number of Roman sites in the region, no data exists on the climatic conditions in the settlements at the time of Roman occupation of Dacia. A lack of climatic proxy records from sites, hampers our understanding of climatic conditions over the RWP in the area. This is particularly important because the only temperature record that exists for Romania comes from a higher altitude area (i.e., Mocearu Lake; Eastern Carpathians)[4] and has low resolution. To assess the direct climatic conditions during the Roman conquest of the Dacian

[1] PATTERSON *et alii* 2010.
[2] HU *et alii* 2022.
[3] PISO 2001.
[4] RAMOS-ROMÁN *et alii* 2022.

territories, we analyzed two sediment samples from the amphitheatre of *Colonia Dacica Sarmizegetusa* site. Using organic geochemistry (i.e., biomarkers) we reconstruct mean annual air temperatures, soil pH and BIT index based on branched GDGTs, and carbon preference index, average chain length and grass over trees ratio based on *n*-alkanes, to constrain the short scale climatic conditions in central Romania during the roman presence. Additionally, we have tested the presence of organic lipophilic biomarkers to check if further human-produced biomarkers are preserved in the sediments.

2. ARCHAEOLOGICAL CONTEXT

The archaeological site is located in Sarmizegetusa village, in the western side of Hațeg Basin (Fig 1) and is part of the former *Colonia Dacica Sarmizegetusa*, the first Roman town in Dacia, symbolically called the first capital of the province. The amphitheatre was researched during multiple phases (1890 – 1893; 1934 – 1936; 1981 – 1987; 1993 – 1996)[5] and excavated almost entirely until present. Between 2022 and 2024, the research had a preventive character, having as objective the investigation and identification of building structures and the monument evolution during historical time[6].

The site expands over ~35 ha *intra-muros* and another 60 – 80 ha outside of the protection walls[7]. The amphitheatre is located ~110 m north outside of the city walls, close to the northern gate, sacred area and the provincial altar dedicated to the cult of the emperors (Fig 2). In the vicinity, next to the eastern gate, a sanctuary dedicated to the goddess Nemesis was discovered as well[8].

3. ARCHITECTURAL ELEMENTS AND STRATIGRAPHY

3.1. Amphitheatre

The amphitheatre is combining elements of mainly type II and some of type I construction typology (i.e., cassettes filled with soil, above which were placed the stone tribunes – *cavea*) (Fig 2). It was built in two phases: a simpler one dated ~108 AD and a later more complex one around 158 AD[9]. During the first phase the arena wall and the two lodges were built (i.e., *pulvinaria* and *suggesta*), one on the northern side and the other one on the southern side. The base was made of stone, with wood tribunes supported on wooden pillars, traces of them (post-holes) being identified all around the amphitheater during the excavation[10]. This phase is considered contemporary with the foundation of the city. A second phase is marked by adding two stone concentric circles, held together by transversal walls.

The dimensions are 88 × 69 m and 66 × 47 m for the arena. With a capacity of 5000 places, Sarmizegetusa amphitheatre was one of the largest buildings of its type in the Dacian territory (Fig 2). The long ax is oriented E – W, along the road that joined Tibiscum and Apulum cities and passing through Sarmizegetusa. The *cavea* is narrow, sitting on the stone foundation. The main entrances are at the ends of the long ax, the eastern one probably being the official access point (i.e., *porta pompae*) due to its proximity to the mentioned temple). On the short ax there were placed two secondary entrances, and twelve other small ones along the exterior wall, allowing supplementary access to spaces below the tribunes.

3.2. Sewage

During the 2022 archaeological excavation of the arena, a channel (C1; Fig 2) was discovered in the southeastern side, with SW – NE direction. The channel measuring 40 depth and 25 cm wide was covered with schist slabs and had a length of ~21 m. The channel itself was made with the same rock fragments (quarried nearby) with yellow clay mortar, a total of five layers. Spaces were filled with smaller rocks or brick fragments. The covering slabs were also fixed over a layer of mortar. The channel base is irregular, carved directly in the soil, allowing the water to infiltrate faster. The interior of the channel was filled with sediments with two distinct layers: a dark layer in the lower half and a yellowish layer in the upper part (Fig 6). The lower layer contains fragments of charred material. Samples analyzed in this study were collected from both layers, from the central part of the filling (Fig 7). The role of this channel was interpreted as collecting pluvial water, retrieving the excess from another channel orientated W – E and it was later decommissioned, possibly due to filling. Based on the architecture of the channel and the amphitheater, we overall correlate the filling with the period of operation of the construction phases[11].

4. MATERIALS AND METHODS

4.1. Lipids extraction and analysis for environmental data

Two sediment samples were collected from the filling of the sewage channel, one per layer. Samples were dried at room temperature, weighed, and manually ground. Lipids were extracted using a Soxhlet apparatus with a mixture of dichloromethane (DCM) and methanol (MeOH) 7.5:1 (*v:v*) in pre-extracted cellulose thimbles. Extracts were evaporated to near dryness under continuous N_2 flow using a TurboVap LV. Elemental Sulphur was removed from the total lipid extracts (TLE) using Cu shreds activated with 10% HCl. The vials containing TLE, activated Cu and magnetic rods were placed on a rotary table for ~20 hours. The TLEs were further filtered over a Na_2SO_4 column to remove Cu fragments, water and other residues. The remaining solvents were evaporated using N_2. The desulphurization was repeated until no reaction with the Cu was observed. TLE was finally separated into three fractions containing different lipids using Al_2O_3 column chromatography. Fraction 1 was eluted by using 4 ml solvent mixture of *n*-hexane (HEX) and DCM (9:1, *v:v*). Fraction 2, containing ketones, was eluted by using 4 ml DCM, while fraction 3, containing the polar fraction

[5] ALICU 1997.
[6] ȚENTEA *et alii* 2025.
[7] PISO 2001; PISO 2017.
[8] ALICU 1997; PISO 2001; PISO 2017.
[9] ALICU 1997.
[10] ȚENTEA *et alii* 2025.
[11] ȚENTEA *et alii* 2025.

including the glycerol dialkyl diglycerol tetraethers (GDGTs), was eluted using 4 ml of DCM:MeOH (1:1, *v:v*) based on the laboratory protocol used at Senckenberg Biodiversity and Climate Research Centre (SBiK-F), Frankfurt am Main Germany[12].

The polar fraction containing glycerol dialkyl glycerol tetraether lipids (GDGTs) was dissolved in a 1ml mixture of *n*-hexane (*n*-hex)/isopropanol (IPA)-(99:1, *v:v*) and slightly dispersed using an ultrasonic bath (~10s/sample), then filtered over a 0.45 mm PTFE filter using a 1 ml syringe. Polars were measured using a Shimadzu HPLC, using two UHPLC silica columns (2.1 × 150 mm, 1.7 µm) in series, connected to a 2.1 × 5 mm pre-column coupled to an ABSciex 3200 QTrap chemical ionization mass spectrometer (HPLC/APCIeMS) at SBiK-F. Column temperature was 30 °C and flow rate was 0.2 ml/min. GDGTs were eluted isocratically using 18% B for 25 min, then a linear gradient to 35% B in 35 min, followed by a ramp to 100% B in 30 min, where B is hexane/isopropanol (9:1; *v:v*) and A is hexane. For each sample a 5 µl injection volume was used and GDGT detection was achieved through single ion monitoring. Branched GDGTs quantification was performed using the Analyst software and the peaks were integrated manually for each sample (Fig 7 A).

The apolar fraction containing *n*-alkanes was measured using the Gas Chromatography-Mass Spectrometry (GC-MS) at SBiK-F using a ThermoScientific Trace GC Ultra – DSQII equipped with a HP–5MS column (30 m × 0.25 µm × 0.25 µm). The GC oven was held at 70 °C for 1 minute, ramped at 10 °C/minute to 180 °C (5 minutes hold), then ramped at 3 °C/minute to 320 °C (15 minutes hold). *n*-Alkanes were identified by comparing their retention time and mass spectrum to an external standard (*n*-C_7 to *n*-C_{40}; Supelco) and quantified using peak areas calibrated against the corresponding standard peak (Fig 7 B). Peak assessment and quantification were performed using the Thermo Xcalibur 2.2 SP1.48 software.

4.2. Lipids extraction and scan for organic lipophilic biomarkers

One sample of the filling of a sewage canal (SAR 1) was selected to track the presence of organic lipophilic biomarkers, such as steroidal compounds (Fig 8). The sample was dried in the oven at 60 °C overnight, weighed and after addition of internal standard 5α-cholestane (0.1% solution) was Soxhlet extracted using a mixture of chloroform/MeOH (2:1; *v/v*) for 8 hours at Nuclear Physics Institute of the CAS in Prague. Before tracking the possible steroidal compounds, which demands solid phase extraction into several fractions using different type of extraction mixtures to separate different groups of compounds[13], the sample was separated into neutral and acidic fraction to monitor preserved lipophilic compounds. After extraction, residual solvent was removed, and total extract redissolved in 2 ml of extraction mixture. The TLE aliquot was saponified using 10% solution of KOH in MeOH at 60 °C for 30 minutes. Saponified aliquot was then extracted by a mixture of hexane/diethylether mixture (1:1; *v/v*) to collect the neutral fraction and after HCl treatment to collect the acidic fraction. For GC analyses, an aliquot was taken from both fractions of the sample extracts, evaporated under the stream of inert gas to dryness and derivatized using the derivatization reagent BSTFA (N-O-(bis)trifluoroacetamide) at 70 °C for 1 hour. The excess of derivatization agent was then evaporated to dryness under a stream of inert gas, dissolved in a defined amount of HPLC hexane and injected onto the column in GC-MS. The separation of the compounds was carried out on a Restek Rxi–5MS column with dimensions 30 m × 250 µm × 0.25 µm. An Agilent 8890 gas chromatograph with a Leco TOF flow-through mass spectrometer was used for the analysis. The carrier gas was helium at a flow rate of 1.4 ml min–1. The sample was injected onto the column at 250 °C in split mode (1:50; *v/v*). The temperature program for separation was set at 70 °C for 2 minutes, followed by an increase to 180 °C with a sub-step of 10 °C min^{-1} and a hold time of 15 minutes then with a step of 10 °C to 320 °C with a hold time of 5 minutes.

4.3. GDGT-based temperature calculation and soil pH

4.3.1. Mean annual air temperature (MAAT) and pH

MAAT estimations are based on the relative distribution of brGDGT membrane lipids (Tables 1, 3) originating in the soil from and around the archaeological site, registering the signal during the deposition of each layer. For MAATs and soil pH calculation, we used the calibration of de Jonge[14] where:

MAAT' = 7.17 + (17.8 × GDGT Ia) + (25.9 × GDHT Ib) + (34.4 × GDGT Ic) – (28.6 × GDGT IIa)

pH = 7.15 + 1.59 × CBT'

CBT' is expressed as:

CBT= log10 ((GDGT Ic + GDGT IIa' + GDGT IIb' + GDGT IIc' + GDGT IIIa' + GDGT IIIb' + GDGT IIIc') / (GDGT Ia + GDGT IIa + GDGT IIIa))

where GDGT I – GDGT III are branched GDGTs.

Root Mean Square Error (RMSE) of biomarker-based MAAT is ~4.6 °C.

4.3.2. Mean temperature above freezing (MAF)

MAF represents the mean temperature of the months with a mean temperature above 0°C and is calculated based on the MBT'5ME index, that summarizes the variability in Methylation of 5-methyl Branched Tetraethers[15], using the calibration of Raberg[16].

RMSE of MAF is 2.32°C.

MAF (° C) = – 0.5 + 30.4* MBT' 5ME

MBT' 5ME = ([Ia] + [Ib] + [Ic])/([Ia] + [Ib] + [Ic] + [IIa] + [IIb] + [IIc] + [IIIa])

4.3.3. BIT Index

The BIT (Branched and Isoprenoid Tetraethers) index is a proxy that defines the terrigenous versus aquatic components of the organic matter in sediments. The BIT index is the ratio of the three major brGDGTs (mostly terrigenous) to isoGDGT crenarchaeol (aquatic)[17]:

BIT= [(GDGT-I) + (GDGT-II) + (GDGT-III)] /

[12] VASILIEV 2021. Laboratory notebook for internal use only.
[13] BULL *et alii* 2003.
[14] DE JONGE *et alii* 2014.
[15] DE JONGE *et alii* 2014.
[16] RABERG *et alii* 2021.
[17] HOPMANS *et alii* 2004.

[(crenarchaeol) + (GDGT-I) + (GDGT-II) + (GDGT-III)]

Crenarchaeol is a chemical compound derived from the metabolic activity of the Thaumarchaeota group[18], the most abundant archaea on Earth[19]. Is abundant in aquatic environments but present in smaller amounts also in soils[20]. BrGDGTs occur in high abundances in terrestrial settings, including soils and peats[21]. BIT values close to 1 indicate a predominantly terrigenous source, while low values (close to 0) indicate a strong aquatic source of the organic matter[22]. In continental settings, however, lower values could also be linked to changes in moisture availability or evaporation[23].

4.4. N-alkanes ratios

n-Alkanes were identified using a known external standard mixture (Alk C_7-C_{40} – Supelco 49452-U, 1000 ng/µl) with the Thermo Xcalibur software. To track the *n*-alkanes sources and distribution, average chain length (ACL) and carbon preference index (CPI) were calculated according to Gagosian and Peltzer[24]and Marzi et alii[25], respectively.

$ACL = ((C_{21} \times 21) + (C_{23} \times 23) + (C_{25} \times 25) + (C_{27} \times 27) + (C_{29} \times 29) + (C_{31} \times 31) + (C_{33} \times 33)) / (C_{21} + C_{23} + C_{25} + C_{27} + C_{29} + C_{31} + C_{33})$

$CPI = ((C_{23} + C_{25} + C_{27} + C_{29} + C_{31}) + (C_{25} + C_{27} + C_{29} + C_{31} + C_{33})) / (2 \times (C_{24} + C_{26} + C_{28} + C_{30} + C_{32}))$

The grass-tree ratio was further calculated as the C_{31}/C_{27} *n*-alkane ratio[26].

5. RESULTS

5.1. Calculated temperatures and soil pH

GDGTs were successfully analyzed for two samples, SAR1 (base layer) and SAR3 (top layer). Calculated MAAT values are 11.1°C for SAR1 and 11.8°C for SAR3 (Table 3; Fig 3A), therefore, the average value for the channel filling is 11.4°C. Calculated MAF values are higher than MAATs and are 13.0°C for SAR1 and 12.8°C for SAR3.

Soil pH estimated values correspond to slightly alkaline soils with values of 7.4 for SAR1 and 7.2 for SAR3, with an average value of 7.3 (Table 3; Fig 3A). The pH is following the same trend as MAAT.

5.2. BIT index and n-alkanes ratios

Calculated BIT values for *Colonia Dacica Sarmizegetusa* archaeological site are 0.76 for SAR 1 sample and 0.78 for SAR 3 sample, with an average value of 0.77 (Table 3; Fig 3A)

ACL values are 27.4 for SAR 1 and 28.7 for SAR 3 (Table 3; Fig 3B). CPI value for sample SAR 1 is 2.5, while for SAR 3 it is 0.6. The grass-tree ratio (C_{31}/C_{27}) values are 1.23 for sample SAR 1 and 0.90 for sample SAR 3 (Table 3; Fig 3B). As opposite to ACL, CPI and grass-trees ratio numbers decrease towards the top of the profile.

5.3. Lipids extraction and testing for other lipids

Neutral and acidic fractions were analyzed using GC-MS. Neutral fraction contained linear homologic series of even *n*-alkanes ranging from C_{22} to C_{34} and linear fatty alcohols (Fig 8A) for m/z 75). Acidic fraction contained mainly long and very long chain fatty acids ($C_{20:0}$-$C_{24:0}$), with dominant abundance of palmitic ($C_{16:0}$), stearic ($C_{18:0}$) and unsaturated oleic ($C_{18:1}$) acids (Fig 8B). However, no steroidal compounds were detected in any of the fractions, thus, further solid phase extraction of total lipid extract was not performed.

6. DISCUSSION

Romans conquered Dacia after the two wars led by Emperor Trajan between 101 – 102 and 105 – 106. Soon after, they established a new city that became the first capital of the province. On its full name *Colonia Ulpia Traiana Augusta Dacica Sarmizegetusa*, it took the name of the old Dacian capital Sarmizegetusa Regia, situated approximately 30 km west. Even though much is known about the general archaeological context and the roman expansion timeline in the area, the environmental conditions in the region during this time interval were never researched. Here we are investigating the short-term paleoclimatic conditions at the site location during the roman occupation and discuss the implications of our results on a broader scale to understand how/if climatic conditions influenced the roman expansion in Eastern Europe and beyond.

6.1. Organic matter sources

BrGDGTs (GDGT I to GDGT III) are membrane lipids produced primarily by bacteria originating in soils, peats, lacustrine and deltaic sediments, indicating an overall terrestrial origin[27]. Their terrigenous source and good capacity preservation over time is extremely useful in reconstructing mean annual air temperatures and soil pH[28]. The analyzed samples from Sarmizegetusa register the signal from the soil around the archaeological site, allowing us to reconstruct the climatic conditions in the area during the time of Roman occupation (Fig 3; Tables 1, 3).

n-Alkanes are acyclic saturated hydrocarbon compounds found in the cuticles of vascular plants[29]. Due to their increased resistance against microbial decomposition and age-determined decay in comparison with lipidic precursor compounds like fatty acids and alcohols[30], *n*-alkanes are usually very well preserved in sediments, reflecting the sources of organic biomass in sediments[31] and the vegetation type contributors. *n*-Alkane homologues with chain lengths shorter than C_{21} are derived from aquatic elements such as algae and submerged plants, but also microbial activity. Higher homologues (C_{21} – C_{23}) are preferentially produced by macrophytes, reeds and mosses, while above C_{27} predominantly by herbaceous plants, shrubs and trees[32]. *n*-Alkanes

[18] SINNINGHE DAMSTÉ *et alii* 2002.
[19] PESTER *et alii* 2011.
[20] WEIJERS *et alii* 2007.
[21] HOPMANS *et alii* 2004; PESTER/SCHLEPER/WAGNER 2011.
[22] SCHOUTEN/HOPMANS/SINNINGHE DAMSTÉ 2013.
[23] BAXTER *et alii* 2024.
[24] GAGOSIAN/PELTZER 1986.
[25] MARZI/TORKELSON/OLSON 1993.
[26] SCHWARK/ZINK/LECHTERBECK 2002.
[27] SINNINGHE DAMSTÉ *et alii* 2002; HOPMANS *et alii* 2004.
[28] DE JONGE *et alii* 2014; RABERG *et alii* 2021.
[29] EGLINTON/HAMILTON 1967.
[30] DERRIEN/YANG/HUR 2017.
[31] EGLINTON/HAMILTON 1967; MEYERS 1997.
[32] FICKEN/LI/SWAIN/EGLINTON 2000.

homologues between C_{14} and C_{34} were identified in the samples from Sarmizegetusa (Table 2). Higher homologues (i.e., $>C_{25}$) have as source terrestrial vegetation around the site and are important for the reconstruction of the vegetation. The lower homologues through are most probably derived from mosses, bacteria and algae growing in the sewage, and thus have no importance for the study.

Fatty acids were identified on the site as well, but they are quite ubiquitous in lipid extract of soils[33]. They arise from the decomposition of organic matter, but in this case, it is difficult to assign the source. Given the presence of mixed chain *n*-alkanes, it is possible that some of the fatty acids to be also derived from algae growing inside the sewage. Linear fatty alcohols are also present. Their origin together with alkanes or very long fatty acids probably derives from the decomposition of plant tissues (e.g., cutin or suberin)[34], also indicating a vegetal source. The lack of steroidal compounds supports the hypothesis that the channel was draining pluvial water from around the amphitheater, and not from the inside.

6.2. Regional temperature during the RWP

At Sarmizegetusa Ulpia Traiana MAAT averages 11.4°C for the IInd century AD, two degrees higher than present day 9.5°C at the same location, and ~4°C more than present day Hațeg Basin mean annual temperatures (6 – 8°C). Sarmizegetusa MAAT values are also ~2.5°C higher than the same biomarker-based MAAT values at Mocearu Lake (9°C; Eastern Carpathians), but close to Mocearu MAF values (~12°C)[35]. The close MAAT and MAF values for Sarmizegetusa (~500 m elevation) indicate warmer and more stable temperatures in the Hațeg Basin for the analyzed interval, in comparison to the Eastern Carpathians (780 m elevation at Mocearu Lake).

Other available records from Romania also indicate warmer and drier conditions for the Roman period. The precipitation curve from Cloșani Cave (Southwestern Carpathians; ~50 km south of Sarmizegetusa)[36] indicates a decrease in precipitations after 50 AD (from ~75 to ~30 mm), while testate amoebae abundance in Lake Iaz core (Western Carpathians)[37] register a major decrease, indicating an important level drop down until ~300 AD (Fig 4). The total mineralogenic matter content in Șureanu peat bog (Southern Carpathians)[38] (Fig 4) also indicates a drying of the mire during the roman presence in Dacia, as well as the Titanium (Ti) content in Lake Ighiel (Northwestern Carpathians)[39]. pH and BIT index values from Sarmizegetusa are also supportive of increased evaporation (pH ~7.3; BIT values of 0.7) in the soil and aridity (Fig 3A).

Our *n*-alkanes data show a higher abundance of long chain *n*-alkanes in the sediment collected from the lower layer at Sarmizegetusa, particularly C_{27} and C_{29} (more abundant in trees and shrubs; Fig 3B), followed by a decrease to almost half for the upper layer, indicating a decrease in waxes coming from woody plants, and thus in tree coverage around the site. Chared material and arboreal pollen from Oltina Lake[40] indicate a strong increase in burning mass for the roman period at the Lower Danube (particulary between 2000 – 1700 BP; Fig 4) over major tree coverage decreasing, suggesting an increase in the fire regime, as well as an important demand of wood for this time period. Pollen data from Avrig 1 core (S. Transylvania)[41], also show a low percentage of *Quercus* and a dominance of *Carpinus* pollen in the area, a more open space taxon. Even though Oltina Lake charcoal and pollen fluxes show an important usage of wood for the roman period in general[42], after 100 AD (when romans conquered Dacia), there is a short increase in tree coverage/decrease in charcoal, perhaps due to part of the army/population mobilization from the *Danubian limes* to the *Dacian limes*. Based on the available records, we observe an overall combined environmental effect for the roman presence in Romania, generally induced by the natural warming and locally by human activity, effect that led to a decrease in forested areas in central and southern Romania (i.e., Dacia and Moesia provinces).

On a continental scale, the long-term European climate driver for Holocene (that includes the RWP) is the North Atlantic Oscillation (NAO) which modulates the North Atlantic storm track, controlling precipitations and temperature over the continent. The positive phase of NAO (NAO^+) is responsible for low precipitation rates and milder winters over southern and Eastern Europe, while the negative phase (NAO^-) is characterized by a wetter regime. Europe was under a short NAO^+ phase between 100 and 200 AD[43] (Fig 5), resulting in drier and warmer conditions in the study area. This period coincides with the maximum expansion of the Roman Empire and subsequently with the roman presence in Dacia. The paleoclimate data from Sarmizegetusa archaeological site (this contribution), as well as other Romanian records[44] (Fig 5) indicate warmer conditions during this period, that could have favored the displacements of troupes in areas that normally have harsher climatic conditions (e.g., the Carpathian-Balkan area, Great Britain, etc.).

6.3. Climatic conditions across the Roman Empire

Available data from different records across the Roman Empire (Fig 5) show similar conditions as in Romania and Eastern Europe. The deposition rate of calcium (Ca) in Roaring Cave in Scotland[45] shows a decrease in the growth rate for the Roman Warming Period, particularly around 1900 BP (i.e., 100 AD; Fig 5). BrGDGTs based MAATs from Lake Sant Front (France)[46] show an increase as well, with maximum being registered between 2000 – 1700 BP (~10°C), as well as pollen based MAATs from Canroute record

[33] RUESS/CHAMBERLAIN 2010.
[34] RIEDERER *et alii* 1993.
[35] RAMOS-ROMÁN *et alii* 2022.
[36] WARKEN *et alii* 2018.
[37] DIACONU *et alii* 2016.
[38] LONGMAN *et alii* 2017.
[39] HALIUC *et alii* 2017.
[40] FEURDEAN *et alii* 2021.
[41] TANȚĂU *et alii* 2006.
[42] FEURDEAN *et alii* 2021.
[43] OLSEN/ANDERSON/KNUDSEN 2012.
[44] TANȚĂU *et alii* 2006; OLSEN/ANDERSON/KNUDSEN 2012; DIACONU *et alii* 2016; LONGMAN *et alii* 2018; EURDEAN *et alii* 2021; RAMOS-ROMÁN *et alii* 2022.
[45] BAKER *et alii* 2015.
[46] MARTIN *et alii* 2020.

(southern France)[47], similar to the MAAT average value for *Colonia Dacica Sarmizegetusa* site of ~11.4°C.

An important increase in the temperature values is also recorded in the marine environment, the Aegean Sea surface temperature values (SST) increasing up to 16°C during the analyzed time interval[48]. $\delta^{18}O$ in Soreq[49] and Jeita cave records[50] (Fig 5) show an important drying trend from 2000 to 1800 AD, indicating a major decrease in humidity in Israel, Lebanon and the Levantine area in general for this time interval. Furthermore, northern Africa is registering a peak in continental aridity (index close to 1 at Cape Ghir, Morocco)[51] and drought (rainfall index close to –1; Chaara Cave, Morocco)[52], indicating warm, dry and evaporitic conditions for the Mediterranean-North African domain. The north hemisphere temperature anomaly[53] shows a value of ~0.2 for the interval between ~2000 – 1700 BP, under positive NAO[54]. C_{31}/C_{27} ratio from Sarmizegetusa site shows an increase in grassy elements during the Roman occupation (Fig 3), indicative of a drier and more open habitat around the site. The ACL values also show a dominant terrestrial signal and a decrease in moisture available for plants (Fig 3).

The cumulated data for the northern hemisphere indicate an overall increase in temperature and evaporation. The similarity in values, even with different proxies, together with the cross-continental distribution of records, shows that the change (i.e., a warmer, drier climate) is not local, but it impacts the entire northern hemisphere. This significant warming overlaps with the maximum expansion of the Roman Empire, with campaigns in Northern and Eastern Europe, North Africa and Asia. Taking into consideration the large extent of the data, we suggest that the milder climatic conditions could have contributed to the Roman expansion towards new territories, colder in normal Holocene conditions.

CONCLUSIONS

The biomarker data from *Colonia Dacica Sarmizegetusa* site is the first paleoclimatic reconstruction from a Roman archaeological site in Eastern Europe, placing the site in the middle of the Roman Warming Period. The calculated MAATs for the site (11.1°C and 11.8°C) indicate an overall 2°C warmer climate than the present day, under a positive NAO influence. The high temperatures are accompanied by a decrease in high taxa *n*-alkanes and an increase in grassy elements, indicating an increased deforestation around the site location. The deforestation is observed in other areas of Romania during the Roman occupation, indicating additional anthropic input. The overall data from Sarmizegetusa show a warmer and drier environment in Eastern Europe during this time interval, similar to various other proxies across Europe, Africa, the Mediterranean and Middle East, indicating that the warming affected a much larger scale territory. This climatic event overlaps with the maximum expansion of the Roman Empire, including the conquest of Dacia. We suggest that the general warming and drier conditions during the RWP could have facilitated the Roman expansion in areas like present day Romania, with harsher weather in normal conditions, particularly during the winter.

[47] D'OLIVEIRA *et alii* 2023.
[48] KONTAKIOTIS 2016.
[49] GRANT *et alii* 2012; BURSTYN *et alii* 2019.
[50] VERHEYDEN *et alii* 2008; CHENG *et alii* 2015.
[51] HOLZ *et alii* 2007.
[52] HU *et alii* 2022.
[53] LJUNGQUIST 2010.
[54] OLSEN/ANDERSON/KNUDSEN 2012.

ACKNOWLEDGEMENTS

The fieldwork research was possible with funds from INP–25 Project, C.J. Hunedoara nr. 2454/202 *"Conservation and preservation of the amphitheatre from the Ulpia Traiana Sarmizegetusa archaeological site"* awarded to the National Institute of Patrimony (Bucharest Romania). The laboratory work was supported by Senckenberg BIK-F and Eberhard Karls Universität of Tübingen. We thank Ulrich Treffert for laboratory support in Frankfurt am Main.

REFERENCES

ALICU 1997
Alicu, D., Ulpia Traiana Sarmizegetusa. Amfiteatrul I (Cluj-Napoca: Muzeul Național de Istorie a Transilvaniei).

BAKER *et alii* 2015
Baker, A. C./Hellstrom, J./Kelly, B. F. J./Mariethoz, G./Trouet, V., A composite annual-resolution stalagmite record of North Atlantic climate over the last three millennia, *Scientific Reports* 5, 10307.

BAXTER *et alii* 2024
Baxter, A. J./Peterse, F./Verschuren, D./Maitituerdi, A./Waldmann, N./Sinninghe Damsté, J. S., Disentangling influences of climate variability and lake-system evolution on climate proxies derived from isoprenoid and branched glycerol dialkyl glycerol tetraethers (GDGTs): the 250kyr Lake Chala record, *Biogeosciences* 21, 2877–2908. https://doi.org/10.5194/bg–21–2877–2024

BULL *et alii* 2003
Bull, I. D./Elhmmali, M. M./Roberts, D./Evershed, R. P., The application of steroidal biomarkers to track the abandonment of a Roman wastewater course at the Agora (Athens, Greece), *Archaeometry* 45, 149–61.

BURSTYN *et alii* 2019
Burstyn, Y./Martrat, B./Lopez, J. F./Iriarte, E./Jacobson, M. J./Lone, M. A./Deininger, M., Speleothems from the Middle East: An Example of Water Limited Environments in the SISAL Database, *Quaternary* 2 (16). Doi:10.3390/quat2020016.

CHENG *et alii* 2015
Cheng, H./Sinha, A./Verheyden, S./Nader, F. H./Li, X. L./Zhang, P. Z./Yin, J. J./Yi, L./Peng, Y. B. Rao, Z. G./Ning, Y. F./Edwards R. L., The climate variability in northern Levant over the past 20,000 years, *Geophysical Research Letter* 42, 8641–8650, doi:10.1002/2015GL065397.

DE JONGE *et alii* 2014
De Jonge, C./Hopmans, E. C./Zell, C. I./Kim, J. – H./Schouten, S./Sinninghe Damsté, J. S., Occurrence and abundance of 6-methyl branched glycerol dialkyl glycerol tetraethers in soils: Implications for palaeoclimate reconstruction, *Geochimica et Cosmochimica Acta* 141, 97–112.

DERRIEN/YANG/HUR 2017
Derrien, M./Yang, L./Hur, J., Lipid biomarkers and spectroscopic indices for identifying organic matter sources in aquatic environments: A review, *Water Research* 112, 58–71. https://doi.org/10.1016/j.watres.2017.01.023

DIACONU *et alii* 2016
Diaconu, A.-C./Grindean, R./Panait, A./Tanțău, I., Late Holocene palaeohydrological changes in a Sphagnum peat bog from NW Romania based on testate amoebae, *Studia UBB Geologia* 60 (1), 21 – 28.
D'OLIVEIRA *et alii* 2023
D'Oliveira, L./Dugerdil, L./Ménot, G./Evin, A./Muller, S. D./Ansanay-Alex, S./Azuara, J./Bonnet, C./Bremond, L./Shah, M./Peyron, O., Reconstructing 15000 years of southern France temperatures from coupled pollen and molecular (branched glycerol dialkyl glycerol tetraether) markers (Canroute, Massif Central, *Climate of the Past* 19, 2127–2156. https://doi.org/10.5194/cp–19–2127–2023
EGLINTON/HAMILTON 1967
Eglinton, G./Hamilton, R. J., Leaf Epicular Waxes, *Science* 156, 1322–1335.
FEURDEAN *et alii* 2021
Feurdean, A./Grindean, R./Florescu, G./Tanțău, I./Niedermeyer./E. M./Diaconu, A. C./Hutchinson, S. M./Nielsen, A. B./Sava, T./Panait, A./Braun, M./Hickler, T., The transformation of the forest steppe in the lower Danube Plain of south-eastern Europe: 6000 years of vegetation and land use dynamics, *Biogeosciences* 18, 1081–1103. https://doi.org/10.5194/bg–18–1081–2021
FICKEN/LI/SWAIN/EGLINTON 2000
Ficken, K. J./Li, B./Swain, D. L./Eglinton, G., An *n*-alkane proxy for the sedimentary input of submerged/floating freshwater aquatic macrophytes, *Organic Geochem*istry 31, 745–749.
GAGOSIAN/PELTZER 1986
Gagosian, R. B./Peltzer, E. T., The importance of atmospheric input of terrestrial organic material to deep sea sediments, *Organic Geochemistry* 10, 661–669. doi:http://dx.doi.org/10.1016/S0146–6380(86)80002–X
GRANT *et alii* 2012
Grant, K. M./Rohling, E. J./Bar Matthews, M./Ayalos, A./Medina-Elizalde, M./Ramsey, C.B./Satow, C./Roberts, A.P., Rapid coupling between ice volume and polar temperature over the past 50,000 years, *Nature* 491, 744–747.
HALIUC *et alii* 2017
Haliuc, A./Vereș, D./Brauer, A./Hubay, K./Hutchinson, S. M./Begy, R./Braun, M., Palaeohydrological changes during the mid and late Holocene in the Carpathian area, Central-Eastern Europe, *Global and Planetary Change* 152, 99–114. https://doi.org/10.1016/j.gloplacha.2017.02.010.
HOLZ *et alii* 2007
Holz, C./Stuut, J.-B. W./Henrich, R./Meggers, H., Variability in terrigenous sedimentation processes off northwest Africa and its relation to climate changes: Inferences from grain-size distributions of a Holocene marine sediment record, *Sedimentary Geology* 202, 499–508.
HOPMANS *et alii* 2004
Hopmans, E. C./Weijers, J. W. H./Schefuss, E./Herfort, L./Sinninghe Damsté, J. S./Schouten, S., A novel proxy for terrestrial organic matter in sediments based on branched and isoprenoid tetraether lipids, *Earth and Planetary Science Letters* 224, 107–116. https://doi.org/ 10.1016/j.epsl.2004.05.012
HU *et alii* 2022
Hu, H.-M./Michel, V./Valensi, P./Mii, H.-S./Starnini, E./Zunino, M./Shen, C.-C., Stalagmite-Inferred Climate in the Western Mediterranean during the Roman Warm Period, *Climate* 10, 93. https://doi.org/10.3390/ cli10070093
KONTAKIOTIS 2016
Kontakiotis, G., Late Quaternary paleoenvironmental reconstruction and paleoclimatic implications of the Aegean Sea (eastern Mediterranean) based on paleoceanographic indexes and stable isotopes, *Quaternary International* 401, 28–42.
LJUNGQVIST 2010
Ljungqvist, F. C., A new reconstruction of temperature variability in the extra-tropical northern hemisphere during the last two millennia, *Geografiska Annaler: Series A* 92 (3), 339–351
LONGMAN *et alii* 2017
Longman, J./Ersek, V./Veres, D./Salzmann, U., Detrital events and hydroclimate variability in the Romanian Carpathians during the mid-to-late Holocene, *Quaternary Science Reviews* 167, 78–95. https://doi.org/10.1016/j.quascirev.2017.04.029.
MARTIN *et alii* 2020
Martin, C./Ménot, G./Thouveny, N./Peyron, O./Andrieu Ponel, V./Montade, V./Davtian, N./Reille, M./Bard, E., Early Holocene thermal maximum recorded by branched tetraethers and pollen in Western Europe (Massif Central, France), *Quaternary Science Reviews* 228, 106109, https://doi.org/10.1016/j.quascirev.2019.106109.
MARZI/TORKELSON/OLSON 1993
Marzi, R./Torkelson, B. E./Olson, R. K., A revised carbon preference index, *Organic Geochemistry* 20, 1303–1306. doi:10.1016/0146–6380(93)90016–5
MEYERS 1997
Meyers, P.A., Organic geochemical proxies of paleoceanographic, paleolimnologic, and paleoclimatic processes, *Organic Geochemistry* 27 (5–6), 213–250.
OLSEN/ANDERSON/KNUDSEN 2012
Olsen, J./Anderson, J.N./Knudsen, M.F., Variability of the North Atlantic Oscillation over the past 5,200 years, *Nature Geoscience,* 5, 11, DOI:10.1038/NGEO1589
PATTERSON *et alii* 2010
Patterson, W. P./Dietrich, K. A./Holmden, C./Andrews, J. T., Two millennia of North Atlantic seasonality and implications for Norse colonies, *Proceedings of the National Academy of Science,* USA, 107, 12, 5306 – 5310.
PETERSE *et alii* 2012
Peterse, F./van der Meer, M. J./Schouten, S./Weijers, J. W. H./Fierer, N./Jacckson, R. B./Kim, J.-H./Sinninghe Damsté, J. S., Revised calibration of the MBT-CBT paleotemperature proxy based on branched tetraether membrane lipids in surface soils. *Geochimica et Cosmochimica Acta* 96, 215–229. https://doi.org/10.1016/j.gca.2012.08.011
PESTER/SCHLEPER/WAGNER 2011
Pester, M./Schleper, C./Wagner, M., The Thaumarchaeota: an emerging view of their phylogeny and ecophysiology, *Current Opinion in Microbiology* 14 (3), 300–306. https://doi.org/10.1016/j.mib.2011.04.007
PISO 2001
Piso, I., Colonia Ulpia Traiana Augusta Dacica Sarmizegetusa. Brève présentation et état de recherche, *Transylvanian Review* 10, 2, 2001, 16–37.
PISO 2017
Piso, I., Colonia Dacica Sarmizegetusa. Scurtă Introducere/ Colonia Dacica Sarmizegetusa, Short Introduction. In: Țentea, O./Rațiu, A. (eds.) Sarmizegetusa. Începuturile Daciei Romane. / Sarmizegetusa. The beginning of Roman Dacia (Cluj-Napoca: Mega), 14–19.
RABERG *et alii* 2021
Raberg, J. H./Harning, D. J./Crump, S. E./de Wet, G./Blumm, A./Kopf, S./Geirsdóttir, Á./Miller, G. H./Sepúlveda, J., Revised fractional abundances and warm-season temperatures substantially improve brGDGT calibrations in lake sediments, *Biogeosciences* 18(12), 3579–3603. https://doi.org/10.5194/bg–18–3579–2021

RAMOS-ROMÁN *et alii* 2022
Ramos-Román, M. J./De Jonge, C./Magyari, E./Veres, D./Ilvonen, L./Develle, A.-L./Seppä, H., Lipid biomarker (brGDGT)- and pollen-based reconstruction of temperature change during the Middle to Late Holocene transition in the Carpathians, *Global and Planetary Change* 215, 103859. https://doi.org/10.1016/j.gloplacha.2022.103859
RIEDERER *et alii* 1993
Riederer, M./Matzke, K./Ziegler, F./Kögel-Knabner, I., Occurrence, distribution and fate of the lipid plant biopolymers cutin and suberin in temperate forest soils, *Organic Geochemistry* 20(7), 1063–1076.
RUESS/CHAMBERLAIN 2010
Ruess, L./Chamberlain, P. M., The fat that matters soil food web analysis using fatty acids and their carbon stable isotope signature, *Soil Biology and Biochemistry* 42(11), 1898–1910.
SCHOUTEN/HOPMANS/SINNINGHE DAMSTÉ 2013
Schouten, S./Hopmans, E. C./Sinninghe Damsté, J. S., The organic geochemistry of glycerol dialkyl glycerol tetraether lipids: A review, *Organic Geochemistry* 54, 19–61. doi:10.1016/j.orggeochem.2012.09.006.
SCHWARK/ZINK/LECHTERBECK 2002
Schwark, L./Zink, K./Lechterbeck, J., Reconstruction of postglacial to early Holocene vegetation history in terrestrial Central Europe via cuticular lipid biomarkers and pollen records from lake sediments, *Geology* 30 (5), 463–466. doi: 10.1130/0091–7613(2002)030<0463: ROPTEH>2.0.CO;22002;30;463–466
SINNINGHE DAMSTÉ *et alii* 2002
Sinninghe Damsté, J. S./Schouten, S./Hopmans, E. C./van Duin, A. C. T./Geenevasen, J. A. J., Crenarchaeol: the characteristic core glycerol dibiphytanyl glycerol tetraether membrane lipid of cosmopolitan pelagic crenarchaeota, *Journal of lipid research* 43 (10), 1641–1651. 10.1194/jlr.m200148-jlr200
ȚENTEA *et alii* 2025
Țentea O./Matei-Popescu, F./Streinu, M./Duca, M., The Amphitheatre of Sarmizegetusa (2021–2024), *Cercetări Arheologice*, 32.1 (forthcoming).
VASILIEV 2021
Vasiliev, I., Laboratory notes for the Organic Geochemistry Lab.
VERHEYDEN *et alii* 2008
Verheyden, S./Nader, F. H./Cheng, H. J./Edwards, L. R./Swennen, R., Paleoclimate reconstruction in the Levant region from the geochemistry of a Holocene stalagmite from the Jeita cave, Lebanon, *Quaternary Research* 70 (3), 368–381. DOI: https://doi.org/10.1016/j.yqres.2008.05.004
TANȚĂU *et alii* 2006
Tanțău, I./Reille, M./de Beaulieu, J.-L./Fărcaș, S., Late Glacial and Holocene vegetation history in the southern part of Transylvania (Romania): Pollen analysis of two sequences from Avrig, *Journal of Quaternary Science,* 21 (1), 49–61. https://doi.org/10.1002/jqs.937.
WARKEN *et alii* 2018
Warken, S. F./Fohlmeister, J./Schröder-Ritzrau, A./Constantin, S./Spötl, C./Gerdes, A./Esper, J./Frank, N./Arps, J./Terente, M./Riechelmann, D. F. C./Mangini, A./Scholz, D., Reconstruction of late Holocene autumn/winter precipitation variability in SW Romania from a high-resolution speleothem trace element record, *Earth and Planetary Science Letters* 499, 122–133. https://doi.org/10.1016/j.epsl.2018.07.027
WEIJERS *et alii* 2007
Weijers, J. W. H./Schouten, S./van der Donker, J./Hopmans E. C./Sinninghe Damsté, J., Environmental controls on bacterial tetraether membrane lipid distribution in soils, *Geochimica et Cosmochimica Acta* 71, 703–713. https://doi.org/10.1016/j.gca.2006.10.003

Fig. 1. Map showing the Dacian province in Danubian context (main map) and at Roman Empire scale (medallion, right side). With red circle it's marked *Colonia Dacica Sarmizegetusa*.

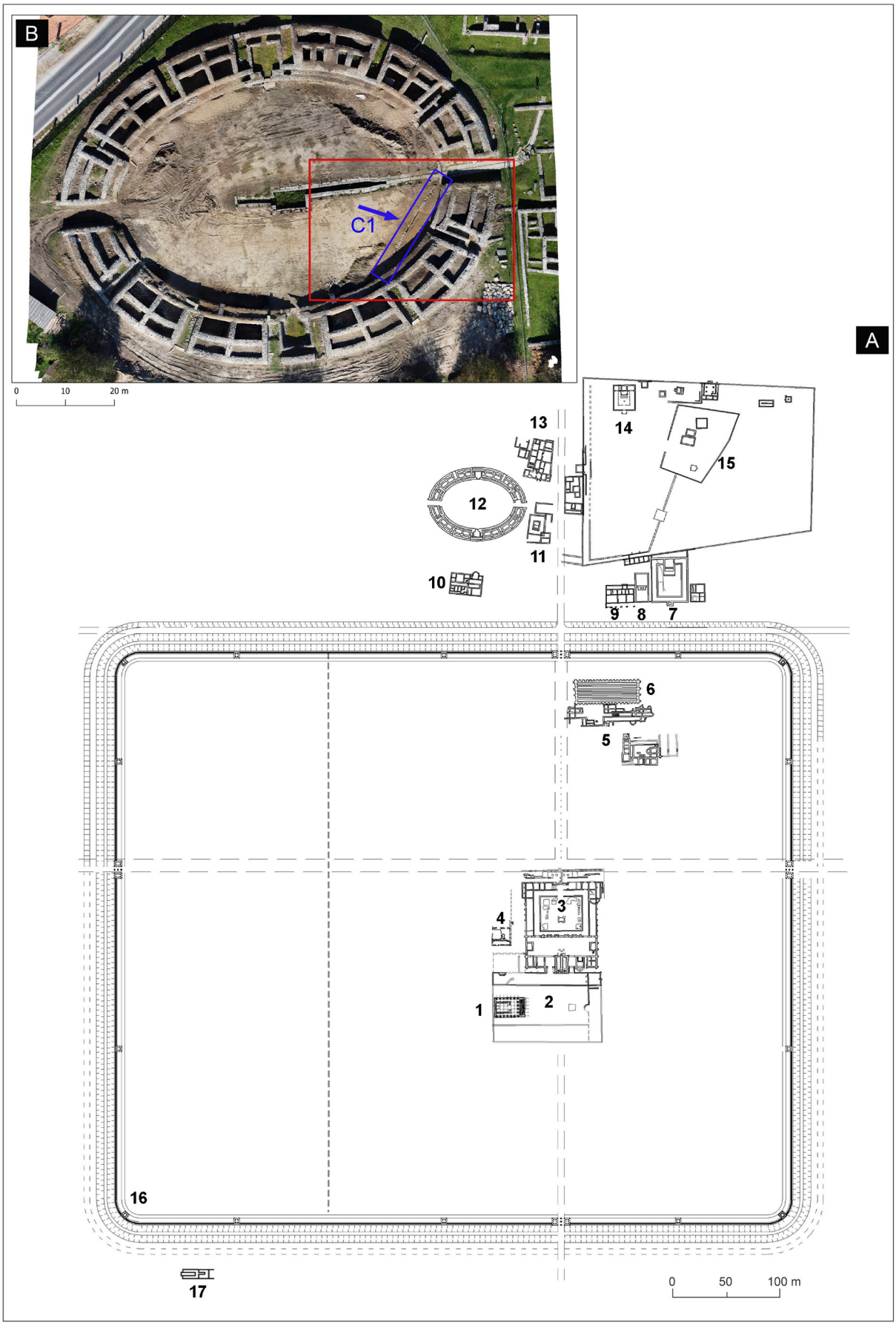

Fig. 2. *Colonia Dacica Sarmizegetusa* excavation plan (A) and detailed amphitheatre (B). In plan A, with numbers, are marked the following main buildings: 1) *Capitolium*; 2) *Forum novum*; 3) *Forum vetus*; 4) *Temple of the Palmyrene gods*; 5) *Domus Procuratoris*; 6) *Horreum*; 7) *The Big Temple*; 8) *Temple of Silvanus*; 9) *Glass Workshop* (?); 10) *Thermae*; 11) *Temple of Nemesis*; 12) *Amphitheatre*; 13) *Schola Gladiatorum*; 14) *Temple of Liber Pater*; 15) *Temple of Aesculapius and Hygia*;16) *Mithraeum*; 17) *Dolichenum*. In plan B the C1 channel is marked with blue.

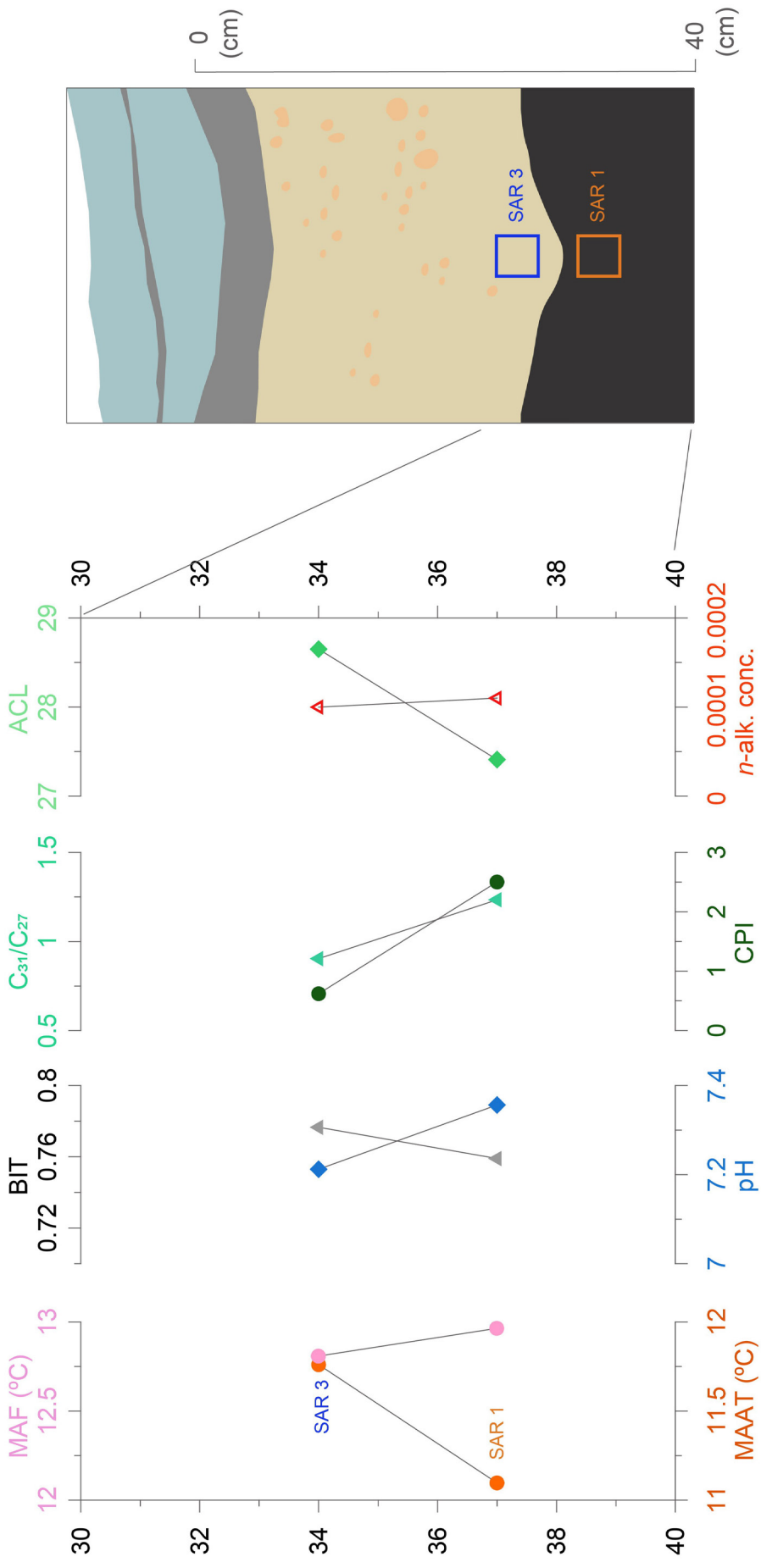

Fig. 3. GDGTs and *n*-alkane derived proxies calculated from the samples collected from C1. MAAT = mean annual air temperature; MAF = mean temperature above freezing; pH; BIT index = branched/isoprenoid tetraether index; CPI = Carbon Preference Index; ACL = Average chain Length; C_{31}/C_{27} = grass/trees ratio and *n*-alkanes concentration.

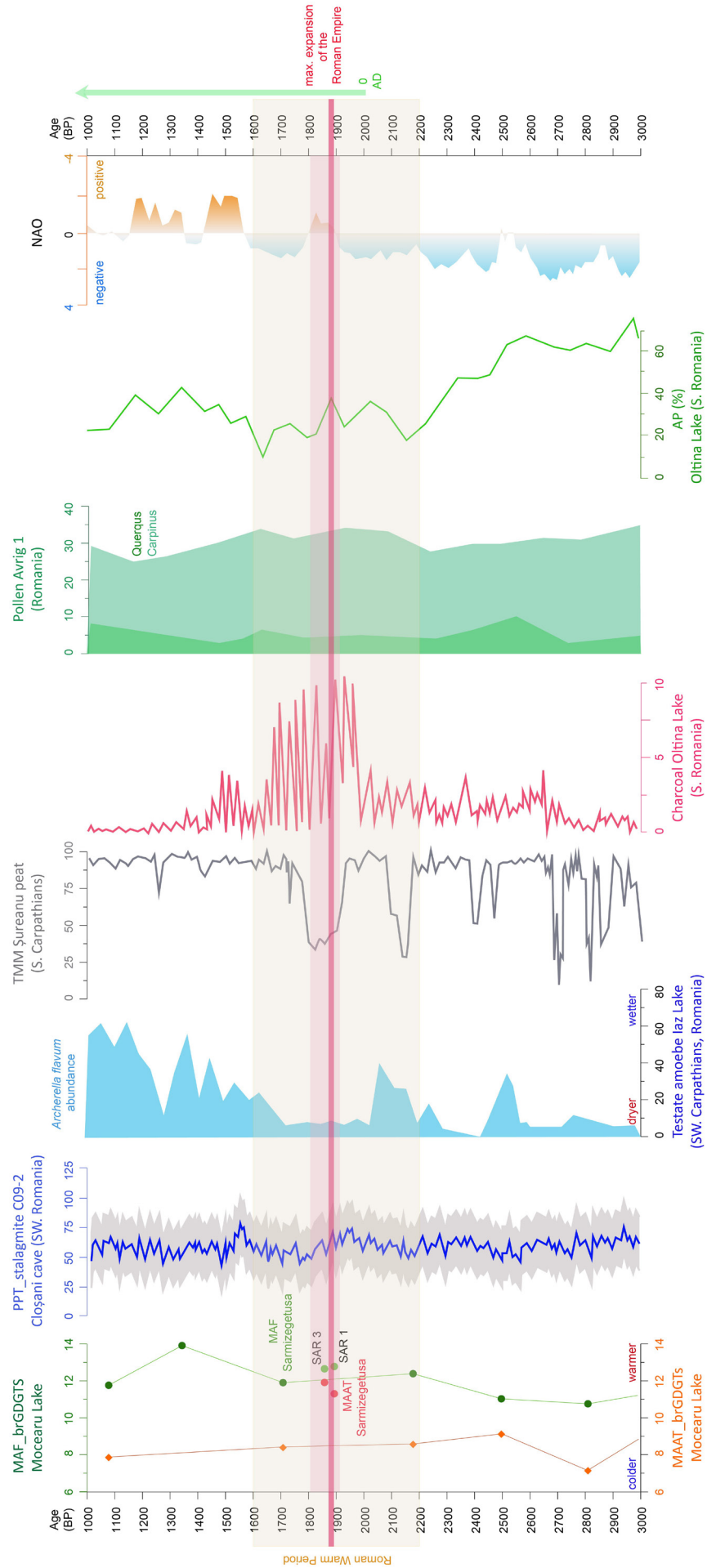

Fig. 4. Paleoclimatic records available for Romania between 3000 and 1000 yr B.P. From left to right: MAF Mocearu Lake; MAAT Mocearu Lake; MAF Sarmizegetusa; MAAT Sarmizegetusa; PPT derived from C09–2 stalagmite in Closani Cave; Testate amoebae abundance from Lake Iaz; TMM from Șureanu peat bog; Charcoal influx from Oltina Lake; Tree pollen% from Avrig 1 core; Pollen% from Oltina Lake; NAO. The orange horizontal band marks the Roman Warming Period, while the red band marks the maximum expansion of the Roman Empire.

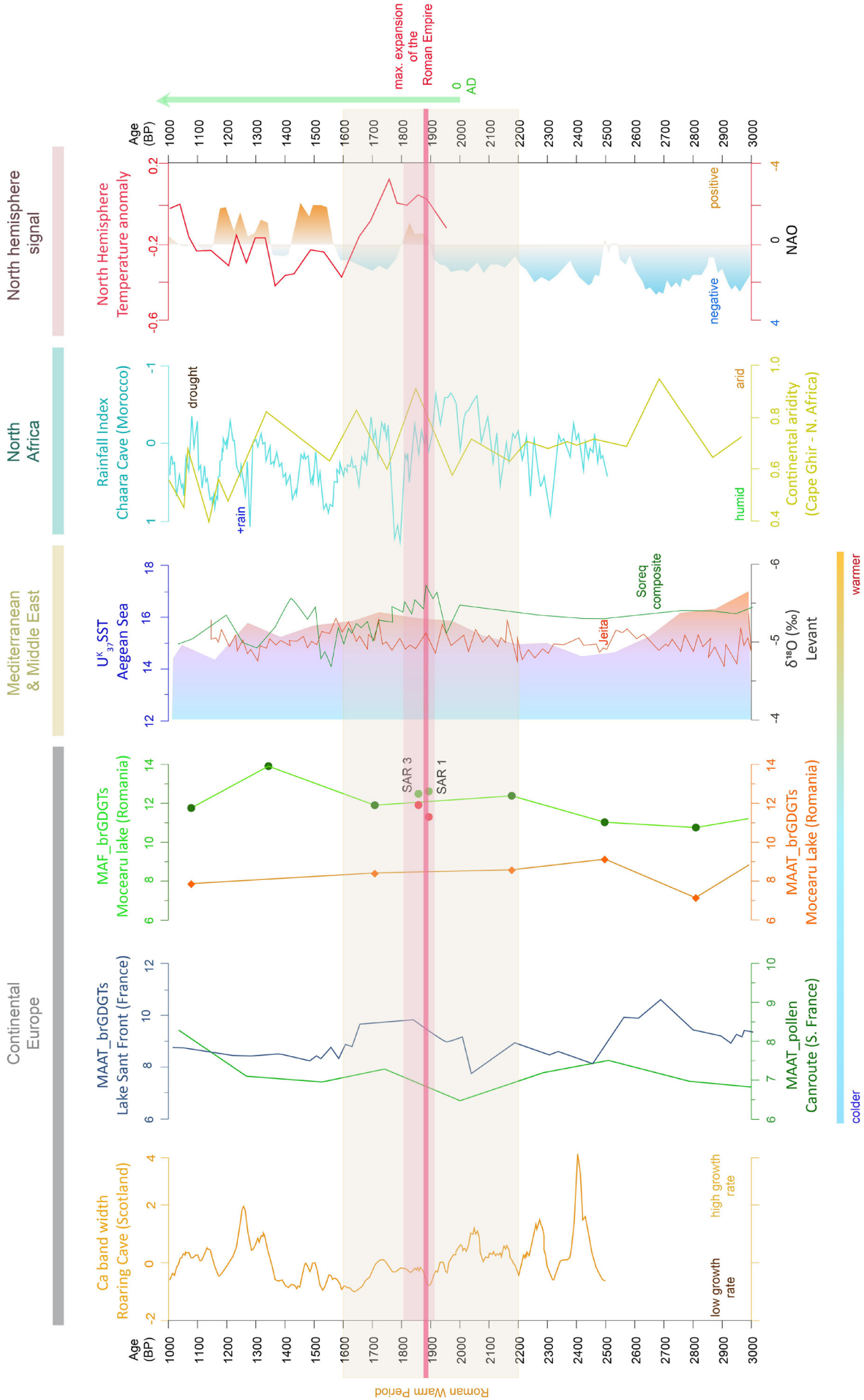

Fig. 5. European and Mediterranean records between 3000 and 1000 yr B.P. From left to right: Calcite precipitation in Roaring Cave; brGDGT-derived MAATs from Lake Sant Front (France) and MAAT pollen-based in Canroute record (France); MAF and MAAT brGDGT-derived in Mocearu Lake (Romania); MAF and MAAT brGDGT-derived from Sarmizegetusa Archaeological Site (Romania); SST based on alkenones in the Aegean Sea (Greece); Rainfall index in Chaara Cave (Morocco); Continental aridity index (Morocco); North Hemisphere Temperature Anomaly Curve; NAO. On the top of the figure, with colored bands, are marked the areas where the groups of records originate. With orange horizontal band is marked the Roman Warming Period, while with red band is marked the maximum expansion of the Roman Empire. On the bottom of the figure is represented the temperature gradient, from colder to warmer.

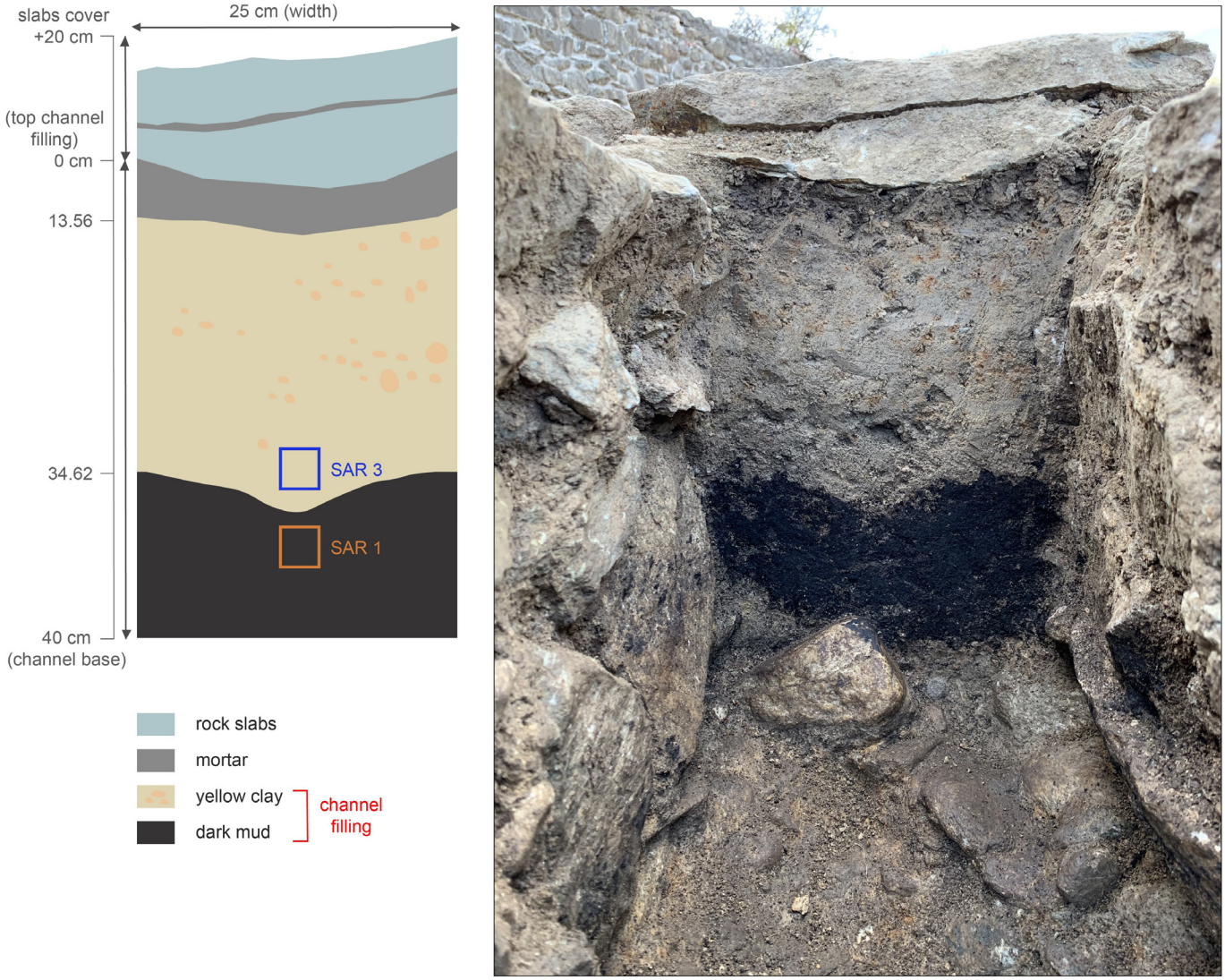

Fig. 6. Stratigraphic column and in-situ picture of the C1 channel filling. With blue and orange squares are marked the two samples analyzed.

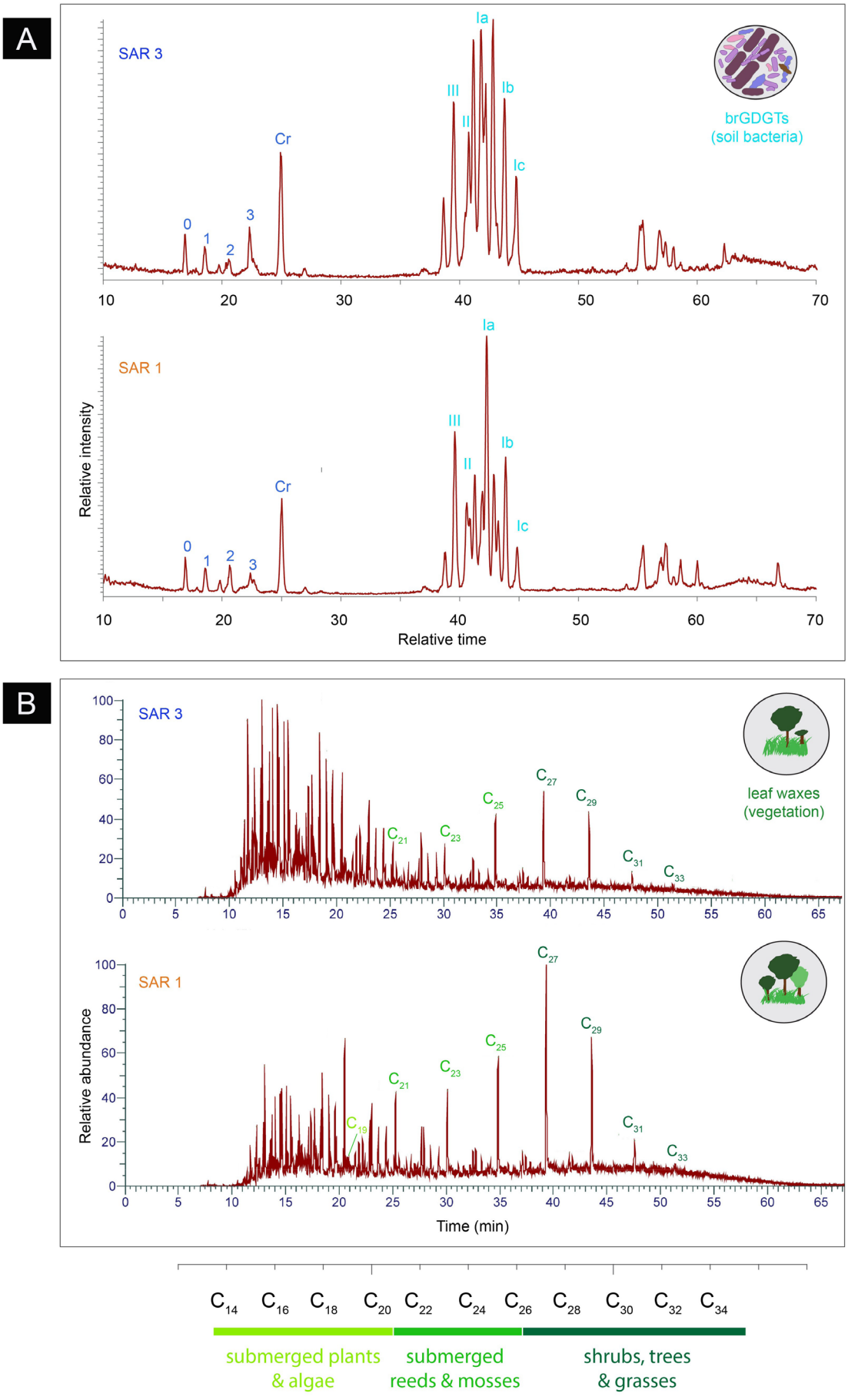

Fig. 7. Chromatograms showing the biomarker distribution in samples. A) Distribution and names of GDGTs for samples SAR 3 and SAR 1. B) Chromatograms showing the *n*-alkanes distribution and sources.

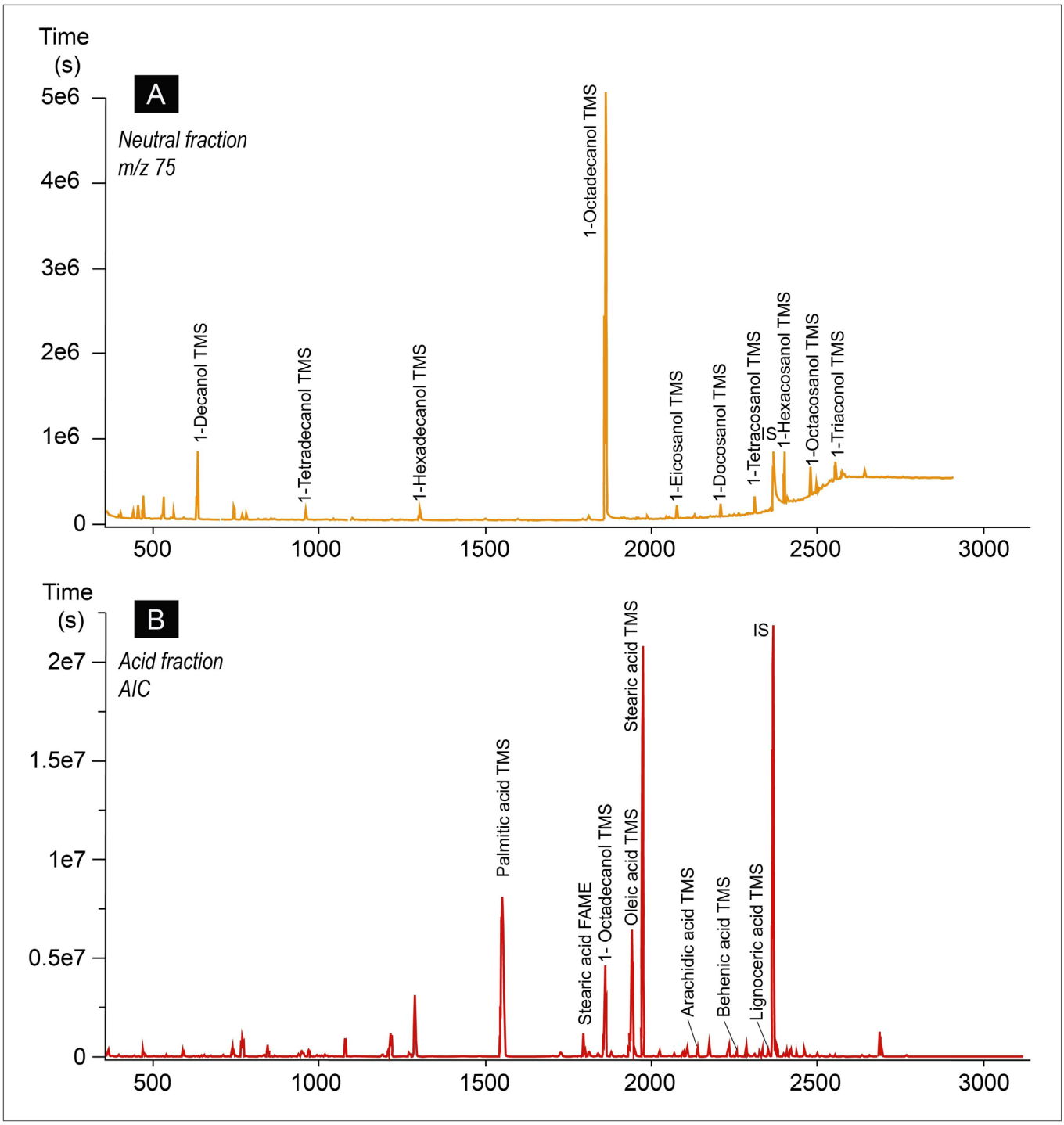

Fig. 8. GC-MS chromatograms of neutral and acidic fractions of SAR 1 sample extract. TMS – trimethyl silyl group, IS – internal standard (5α-Cholestane), FAME – fatty acid methyl ester, AIC – analytical ion chromatogram.

Table 1. brGDGT data.

Sample Name	GDGT-0	GDGT-1	GDGT-2	GDGT-3	GDGT-4	GDGT-4'			iso-GDGTs
SAR1	77200	47100	65000	25200	315000	21200			
SAR3	40900	21200	18600	13400	177000	10900			
SAR1	GDGT-Ia	GDGT-Ib	GDGT-Ic	GDGT-IIa	GDGT-IIa'	GDGT-IIb	GDGT-IIb'	GDGT-IIc	br-GDGTs
	299000	346000	98600	169000	354000	210000	630000	32200	
	GDGT-IIc'	GDGT-IIIa	GDGT-IIIa'	GDGT-IIIb	GDGT-IIIb'	GDGT-IIIc	GDGT-IIIc'		
	154000	524000	75000	244000	22500	55700	3250		
SAR3	GDGT-Ia	GDGT-Ib	GDGT-Ic	GDGT-IIa	GDGT-IIa'	GDGT-IIb	GDGT-IIb'	GDGT-IIc	
	239000	200000	93500	137000	302000	251000	200000	56800	
	GDGT-IIc'	GDGT-IIIa	GDGT-IIIa'	GDGT-IIIb	GDGT-IIIb'	GDGT-IIIc	GDGT-IIIc'		
	43300	239000	24100	53600	6110	16700	3870		
SAR1	Ia	Ib	Ic	IIa	IIa'	IIb	IIb'	IIc	fractional abundance of brGDGTs
	0,092937	0,1075453	0,0306473	0,0525293	0,1100319	0,0652731	0,1958194	0,0100085	
	IIc'	IIIa	IIIa'	IIIb	IIIb'	IIIc	IIIc'		
	0,047867	0,162872	0,0233118	0,0758412	0,0069936	0,0173129	0,0010102		
SAR3	Ia	Ib	Ic	IIa	IIa'	IIb	IIb'	IIc	
	0,128083	0,1071823	0,0501077	0,0734199	0,1618453	0,1345138	0,1071823	0,0304398	
	IIc'	IIIa	IIIa'	IIIb	IIIb'	IIIc	IIIc'		
	0,023205	0,1280828	0,0129155	0,0287249	0,0032744	0,0089497	0,002074		

Table 2. *n*-Alkanes data.

SAR_3	C_{12} area	C_{13} area	C_{14} area	C_{15} area	C_{16} area	C_{17} area	*n*-Alkanes
	2,226E+14	5,405E+14	2,394E+14	1,203E+14	3,728E+14	5,540E+14	
	C_{18} area	C_{19} area	C_{20} area	C_{21} area	C_{22} area	C_{23} area	
	7,938E+14	2,311E+14	1,023E+14	3,323E+14	1,425E+14	1,736E+14	
	C_{24} area	C_{25} area	C_{26} area	C_{27} area	C_{28} area	C_{29} area	
	1,120E+14	1,962E+14	9,152E+14	3,854E+14	6,431E+14	4,547E+14	
	C_{30} area	C_{31} area	C_{32} area	C_{33} area			
	9,550E+14	3,483E+14	4,722E+14	8,956E+14			
SAR_1			C_{14} area	C_{15} area	C_{16} area	C_{17} area	
			1,160E+14	3,943E+14	8,055E+14	2,393E+13	
	C_{18} area	C_{19} area	C_{20} area	C_{21} area	C_{22} area	C_{23} area	
	3,350E+14	1,417E+14	4,855E+14	4,039E+14	4,054E+14	2,756E+14	
	C_{24} area	C_{25} area	C_{26} area	C_{27} area	C_{28} area	C_{29} area	
	2,071E+14	3,603E+14	1,050E+14	5,745E+14	1,007E+14	9,433E+14	
	C_{30} area	C_{31} area	C_{32} area	C_{33} area			
	1,127E+14	7,092E+14	5,948E+14	1,542E+14			

Table 3. BrGDGTs derived, and *n*-alkane based proxies and ratios for *Colonia Dacica Sarmizegetusa* archaeological site.

Stratig-raphy	Sample	SAR 1	SAR 3
	Depth	37 cm	34 cm
GDGTs	MAAT	11,10	11,76
	MAF	12,97	12,81
	pH	7,36	7,21
	BIT	0,76	0,78
	MBT	0,44	0,44
	CBT	0,13	0,04
n-Alkanes	CPI	2,50	0,62
	ACL	27,41	28,65
	C_{31}/C_{27}	1,23	0,90
	n-alk conc. (mg)	0,000	0,000